Effects of electron-hole hybridization on cyclotron resonance in InAs/GaSb heterostructures

C. Petchsingh,* R. J. Nicholas, K. Takashina,† and N. J. Mason
Department of Physics, Oxford University, Clarendon Laboratory, Parks Road, Oxford OX1 3PU, United Kingdom

J. Zeman
L. M. C. I.-C. N. R. S., Grenoble, 25 Avenue des Martyrs, Boîte Postal 166X, F-38042 Grenoble, France
(Received 7 October 2003; revised manuscript received 18 June 2004; published 11 October 2004)

The effect of electron-hole hybridization on the cyclotron resonance of bipolar InAs/GaSb structures is investigated for samples with varying electron-hole coupling. At low magnetic fields it is found that the cyclotron resonance mass of the electrons is significantly enhanced when the electrons and holes are closer together and strongly coupled. A two-band model including electron-hole mixing shows excellent agreement with the experimental results. At higher magnetic fields it is observed that the electron cyclotron resonance line is split into a series of resonances due to electron-hole Landau level hybridization. The magnetic-field positions of these splittings are proportional to the energy separation between the electrons and holes, proving the explanation that they are the result of single-particle coupling. In the quantum limit strong couplings and giant spin splitting of the cyclotron resonance transitions are seen which depend strongly on the exact structure studied.

DOI: 10.1103/PhysRevB.70.155306 PACS number(s): 78.30.Fs, 73.21.Fg

I. INTRODUCTION

The observation of oscillations of the cyclotron resonance mass, amplitude, and linewidth in the semimetallic InAs/GaSb system has provoked a great deal of controversy.[1–7] Current interpretations divide essentially into two possible explanations: electron-hole Bose-Einstein condensation,[2,3,8] and varying degrees of electron-hole hybridization.[3–6,9] To date, experimental evidence has been inconclusive in resolving this debate, though the weight of evidence favors the second explanation.[7,10,11] This paper presents not only further strong evidence supporting electron-hole hybridization as the cause of these oscillations, it also gives a systematic study of the effects of such hybridization on electron effective-mass enhancement and splitting of cyclotron resonance transitions. The strength of the hybridization is experimentally controlled both by varying the InAs well width and by inserting a barrier between the electrons and holes. The experimental results are compared to a simple two-band coupling model including the effect of the minigap that appears where the conduction band and valence band cross. When the barrier is introduced between the electrons and holes all evidence of the electron-hole coupling is removed.

II. THEORETICAL BACKGROUND

A. Type-I nonparabolicity

It is well known that the cyclotron resonance mass can be enhanced relative to the band-edge free carrier mass as a result of conduction band nonparabolicity, with higher energy electrons having a greater effective mass due to interactions with other bands.[12–19] This type of nonparabolicity is identified as type-I nonparabolicity[4] and its effect on the electron cyclotron mass has been shown both theoretically[14,18] and experimentally[17,19] to be dependent on the carrier confinement energy. A three-band formula for the energy dependence of the effective mass m_e^* in a nonparabolic system[19] is given approximately by

$$\frac{m_0^*}{m_e^*} = 1 + 2\frac{\kappa}{E_G}\epsilon, \tag{1}$$

with the nonparabolicity parameter κ=-0.86 for AnAs.[20,21] m_0^* is the band-edge mass, E_G is the energy gap of the bulk InAs which has a value of 418 meV, and $\epsilon = E_0 - E_b + (N+1)\hbar\omega_c$ is the confinement energy of the Nth Landau level, with E_0 and E_b being the ground-state subband energy and the band-edge energy, respectively.

B. Type-II nonparabolicity

In narrow band-gap heterostructures made with materials such as AnAs, it has been reported that type-I nonparabolicity alone is not sufficient to explain the mass enhancement. Theoretical[21,22] and experimental[23] investigations show that tunneling of the electron wave functions into the barrier layers can lead to additional electron effective-mass enhancement and the formation of a minigap. Recent reports on the cyclotron resonance effective mass in bipolar InAs/GaSb systems have included studies of the dependence on layer thickness in InAs/GaSb bilayers,[20,24,25] in InAs/GaSb superlattices,[20,26,27] and in InAs/AlSb/$Al_xGa_{1-x}Sb$ structures,[3,7,28] although none of the previous work has sought to establish clear relationships that might exist between the effective mass and the strength of the electron-hole hybridization. Oscillations of the mass with magnetic field are found to occur which are opposite in phase to those observed due to type-I nonparabolicity and are thus sometimes referred to as antinonparabolicity.[3] This is also referred to elsewhere as type-II nonparabolicity.[4]

The simplest model used to describe the conduction-valence band hybridization and the emergence of minigaps in

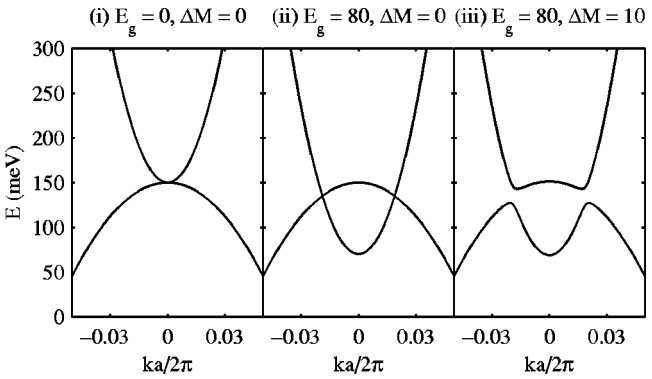

FIG. 1. Calculated electron and hole band dispersions for (i) $E_g=0$, $\Delta M=0$, (ii) $E_g=80$, $\Delta M=0$, (iii) $E_g=80$, $\Delta M=10$ with the atomic spacing $a=6$ Å.

the InAs/GaSb structure considers two bands:[29] the ground electron subband E_0 in the InAs layer, and the ground hole subband H_0 in the GaSb layer. The in-plane dispersion relation is initially assumed to be parabolic and the two states hybridize according to the matrix equation:

$$\begin{pmatrix} E_0 & \Delta M \\ \Delta M & H_0 \end{pmatrix} \begin{pmatrix} \varphi_{E_0} \\ \varphi_{H_0} \end{pmatrix} = E \begin{pmatrix} \varphi_{E_0} \\ \varphi_{H_0} \end{pmatrix}, \tag{2}$$

where $E_0(k)=\hbar^2k^2/(2m_e)$, $H_0(k)=E_g-\hbar^2k^2/(2m_h)$, and E_g is the band gap. The parameter ΔM is related to the size of the minigap, with the minimum energy separation of the bands given by $2\Delta M$. The solutions to this equation are mixed conductionlike and valencelike bands E_C and E_V with energies given by

$$E_C = \frac{1}{2}(H_0 + E_0) + \frac{1}{2}\sqrt{(H_0 - E_0)^2 + 4\Delta M^2}, \tag{3}$$

$$E_V = \frac{1}{2}(H_0 + E_0) - \frac{1}{2}\sqrt{(H_0 - E_0)^2 + 4\Delta M^2}. \tag{4}$$

Figure 1 shows the calculated dispersion relation for the cases (i) $E_g=0$ meV, $\Delta M=0$ meV, (ii) $E_g=80$ meV, $\Delta M=0$ meV, and (iii) $E_g=80$ meV, $\Delta M=10$ meV. The electron mass and the hole mass values, $m_e=0.023\ m_0$ (Ref. 30) and $m_h=0.10\ m_0$,[31] are the values estimated at the band edges. In an ideal parabolic system the electron and hole densities are in equilibrium and therefore the Fermi energy will lie at the crossing point of the two bands. However, the samples studied here are slightly *n* type although the individual layers are not doped. This is due to pinning of the Fermi level by surface states and acceptors in the GaSb layers.[32,33] The Fermi energy will therefore lie slightly above the crossing point of the two bands. Assuming isotropy, the magnitude of the two-dimensional electron and hole densities (N_e, N_h) are given through the standard equations $k_{Fe}=\sqrt{2\pi N_e}$ and $k_{Fh}=\sqrt{2\pi N_h}$, where k_{Fe} and k_{Fh} are the values of k where the Fermi energy E_F crosses the electronlike and holelike segments of the conduction-band dispersion, respectively. N_e and N_h can be determined experimentally via transport measurements, and for a given value of N_e/N_h we can therefore deduce the value of E_F.

C. Cyclotron resonance mass

In the low magnetic field semiclassical limit, the cyclotron resonance mass m^*_{CR} can be expressed in terms of a closed cyclotron orbit in k space with an area A which depends on the cyclotron orbit energy E and the in-plane wave vector magnitude k. The low-field cyclotron mass is given[34] by

$$m^*_{CR} = \frac{\hbar^2}{2\pi}\frac{\partial A}{\partial E}\bigg|_{E=E_F}. \tag{5}$$

In the case of a parabolic dispersion, assuming coaxial and isotropic conduction and valence bands, the cross sectional area A of an orbit is given by πk^2. Using the chain rule, the mass is

$$m^*_{CR} = \hbar^2 k \frac{\mathrm{d}k}{\mathrm{d}E}\bigg|_{k=k_F}. \tag{6}$$

We can thus calculate the cyclotron resonance mass of the conduction (electron) and valence (hole) bands from Eqs. (3) and (4), respectively.

III. EXPERIMENTAL DETAILS

Cyclotron resonance was measured in a farinfrared Fourier transform spectrometer at 2.2 K in the Faraday configuration using unpolarized light with magnetic field up to 14 T. The sample substrates were wedged by 2° to prevent interference distorting the resonance line shape. The resulting transmission spectra were normalized to the spectrum at zero magnetic field, giving a relative spectrum $\tilde{T}=T(B)/T(0)$. Line shapes were fitted to the spectra using the transmission relation given in Refs. 35 and 36, and the effective mass $m^*=eB/\omega_c$ was deduced from the cyclotron energy.

The measurements were performed on two sets of samples, labeled the well width series, and spacer series. All samples were grown by metal organic vapor phase epitaxy on GaAs substrates and consist of a well layer of InAs sandwiched between a 1200 Å GaSb capping layer and a thick (2 μm) GaSb strain-accommodating buffer layer. The structures in the well width series were grown with InAs growth time varying in the range 30–80 s. The growth of the layers was monitored via an *in situ* surface photoabsorption technique.[37,38] The growth rate was estimated from the observation of interference oscillations in the signal as a function of growth time. Assuming a constant growth rate ($\approx$4 Å/s), we estimate that the nominal InAs width w covers the range from 120 Å to 320 Å. Table I lists the samples labeled as *WT* where *T* is the growth time in seconds.

In the spacer series, the coupling between the electrons and holes is controlled by the introduction of short-period superlattices at the interfaces to form a spacer or barrier layer between the InAs well and GaSb. The InAs width was fixed at 240 Å and the number of superlattice periods at the first

TABLE I. The well widths w, carrier densities, and mobilities (μ_e, μ_h) of the samples studied. Densities deduced by cyclotron resonance and given for $B=3$ T for comparison to transport measurements. † denotes N_e estimate based on results at 20 K. ‡ Magnetotransport results for S0−10 indicate the presence of a significant number of holes but simple modelling could not fit the data.

Sample	w (Å)	At interfaces 1st	2nd	N_e by CR (10^{15}m^{-2})	N_e (10^{15}m^{-2})	N_h	μ_e (m^2/Vs)	μ_h
Well width series								
W30	120	-	-	0.63†	0.29	-	1.9	0.68
W35	140	-	-	3.68	1.8	0.84	4.2	1.28
W40	160	-	-	4.27	5.6	4.1	4.4	1.1
W50	200	-	-	7.56	7.6	6.1	7.9	1.0
W60	240	-	-	7.69	7.3	6.2	18.7	0.7
W70	280	-	-	8.47	6.8	6.2	17.5	0.4
W80	320	-	-	7.42	6.0	6.0	26.1	5.9
Spacer series								
S1-1	240	1 SL	1 SL	7.06	6.4	3.4	21.0	1.2
S5-5	240	5 SL	5 SL	6.29	4.7	3.7	9.6	0.5
S10-0	240	10 SL	0 SL	6.68	5.0	4.3	9.1	0.6
S0-10	240	0 SL	10 SL	6.55′	6.5	‡	16.5	‡
S10-10	240	10 SL	10 SL	4.94	4.0	0.5	14.0	0.33

and second interfaces was varied between 0 and 10 periods. Each period of the superlattice consists of 20 Å of InAs and 20 Å of GaSb (5 s growth time each). The narrow layer widths of the superlattices mean that the confinement energies of the electrons and holes are pushed sufficiently far apart in their respective layers that there is a positive energy gap between them. The structure then acts as a barrier, reducing tunneling and mixing effects between the electron and hole wave functions, and their mean spatial separation is increased by the superlattice thickness. The carrier densities and mobilities for the samples in both series have been determined by transport measurements at 4 K (Refs. 39–41) and are also included in Table I for comparison. The electron and hole densities fall off sharply as the well width decreases towards the limiting well width at which the band overlap disappears and the structure becomes semiconducting. The eight-band $\boldsymbol{k}\cdot\boldsymbol{p}$ model predicts this limit to be at ≈90 Å.

IV. RESULTS AND DISCUSSION

A. General observations

Contour plots of the cyclotron resonance spectra for a narrow well sample (W40), an intermediate well sample (W60), a wide well sample (W80), and a sample with ten periods of superlattices at both interfaces (S10-10) are shown in Figs. 2(i), 2(ii), 2(iii), 2(iv), respectively. Darker regions indicate greater absorption within each plot, though shading levels vary between plots: maximum absorption increases from (i) to (iv). Resonances could be observed from both electrons and holes using different spectrometer conditions, however the hole resonances were much more poorly resolved due to both larger linewidths and lower hole densities, and so the study has focussed on the properties of the electrons.

It is seen in all samples that at low magnetic field, typically $B<3$ *T*, the cyclotron resonance is dominated by a single transition peak which is due to the cyclotron motion of the two-dimensional electrons in the InAs well. However, at higher fields the four samples show very different transition features. Sample W40, which has the narrowest well width of the four samples, displays a series of clear transitions with similar slopes, but which are shifted from each other by different offsets. In addition there are a series of weaker transitions with steeper slopes, such as that at 4 T, which breaks off from the electron cyclotron resonance line and increases rapidly in energy as the field increases. This transition is then replaced by another transition which emerges from the low-energy side. A general feature of all of the spectra is that new features appear from the low-energy side replacing those that tail off to the high-energy region. These phenomena resemble observations reported in the literature[6,7,42] and attributed to coupling of the electron and hole bands, but are much more pronounced due to the narrower well widths studied. In the wider well width structures of samples W60 and W80, the spectra have stronger resonance amplitudes due to the greater carrier densities, smaller splittings, and narrower linewidths. The transitions in these samples have similar overall features to those of W40 but the couplings are seen to occur at higher magnetic field and the resonances occur within a smaller envelope around a constant mass value. For comparison, selected transition couplings are indicated in Fig. 2 by (α), (β), and (δ). It is clear that these coupling features have the same pattern and that they shift to higher magnetic field as the well width increases. However, in sample S10-10, with the large spacer layers at both interfaces these coupling features are absent. We note that similar splitting features to those observed in sample W60 are observed in other samples in the spacer series (not shown here), but

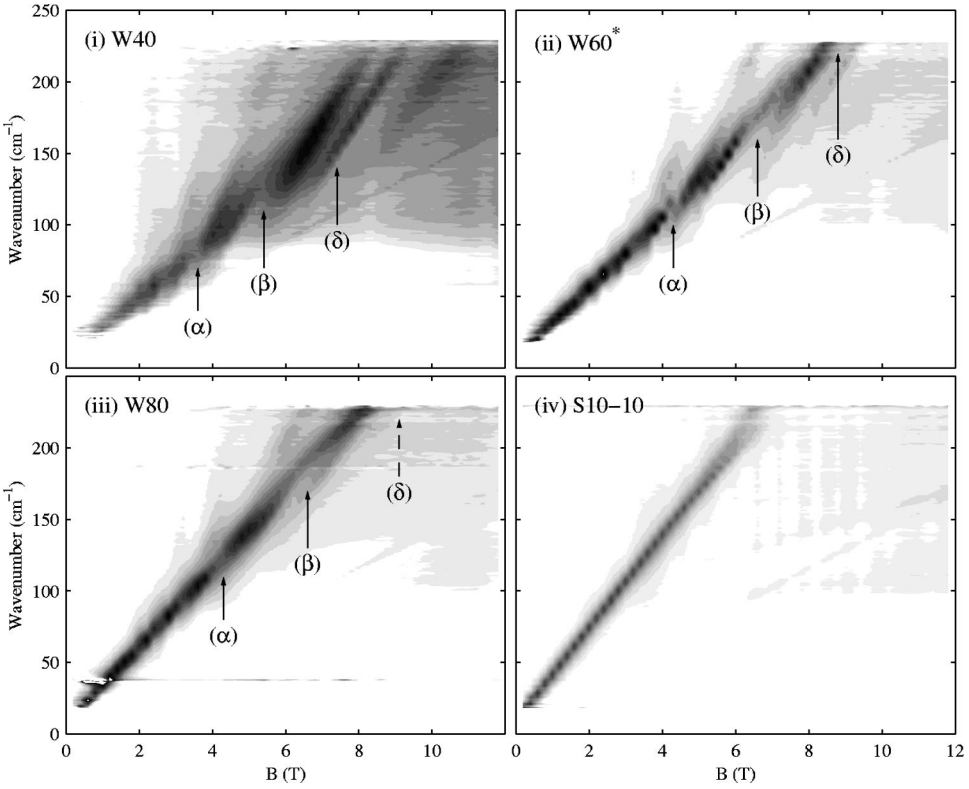

FIG. 2. Contour plots of the cyclotron resonance spectra for samples with different mean electron-hole separations d, ranging from small d in (i) to large d in (iv).

with smaller magnitude. In particular, the features in S10-0 and S0-10 occur at the same fields to within 0.1 T indicating the symmetrical nature of the coupling.

B. Mass enhancement at low field

We now examine the effective mass in the low magnetic field region. The electron cyclotron resonance appears as a single peak with an effective mass $m^*=eB/\omega_c$. Figure 3 shows the transmission spectra at 3 T of all the well width and spacer series samples. We observe that the cyclotron resonance position increases with increasing separation between electron and hole gases. The spectra for all samples appear to be of approximately Lorentzian line shape, but there are clear differences in linewidth and amplitude between them. As the electron-hole separation decreases, the spectrum linewidth generally becomes wider and the transition amplitude reduces. Table II summarizes the values of the cyclotron resonance frequency ω_c, full-width-half-maximum w_L, and intensity I estimated from fitting transmission line

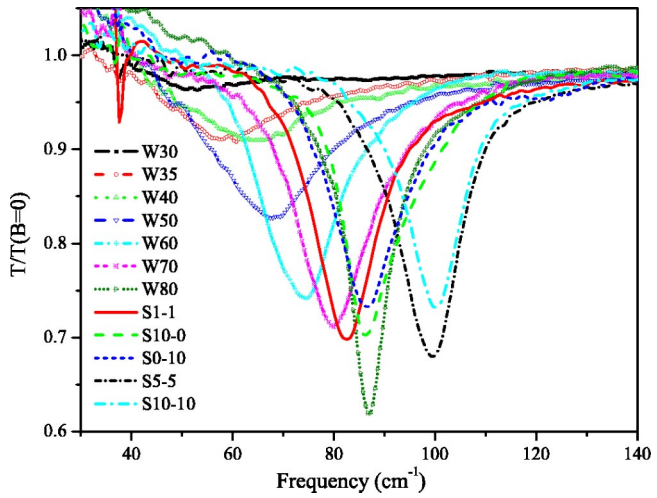

FIG. 3. Cyclotron resonance spectra at 3 T.

TABLE II. The cyclotron resonance fitting parameters: cyclotron frequency (ω_c), full linewidth (w_L), intensity (I), carrier density, and effective mass for the single resonance observed at 3 T for the different samples.

Sample	w (Å)	w_c (cm^{-1})	w_L (cm^{-1})	I	N_c at 3 T (10^{15}m^{-2})	m^* (m_0)
Well width series						
W30	120	56.1	18.4	0.0354	0.63	0.0499
W35	140	60.5	27.2	0.0885	3.68	0.0463
W40	160	65.5	24.7	0.0914	4.27	0.0428
W50	200	68.2	24.4	0.174	7.56	0.0411
W60	240	74.2	16.8	0.260	7.69	0.0378
W70	280	80.5	17.8	0.291	8.47	0.0348
W80	320	87.2	11.6	0.381	7.42	0.0321
Spacer series						
S1-1	240	82.9	14.1	0.303	7.06	0.0338
S5-5	240	99.0	14.5	0.321	6.29	0.0283
S10-0	240	86.4	14.7	0.279	6.68	0.0323
S0-10	240	87.2	15.9	0.268	6.55	0.0321
S10-10	240	100.0	13.8	0.268	4.94	0.0280

shapes at 3 T. The carrier densities and effective masses shown are deduced from the fitted parameters. We see that in the well width series the electron density decreases as the well width decreases due to the increase of the confinement energy in the InAs well, in broad agreement with the values deduced from transport (Table I). By contrast, the spectral linewidth, corresponding to the electron scattering rate, is generally higher for narrower wells.

For narrowing well width (decreasing electron-hole separation), the spectra show a consistent marked increase of the effective mass. The smallest separation, corresponding to a narrow well width of 120 Å (d=90 Å), shows an effective mass of m^*=0.050 m_0, while the addition of ten period superlattices at the interfaces (d=550 Å) sees this fall to m^* =0.028 m_0, which is only slightly higher than the bulk InAs band-edge mass.

1. Well width series

Type-I nonparabolicity predicts increasing cyclotron resonance mass with decreasing well width.[18] An approximation using the analysis of Warburton *et al.*[19] is given in terms of electron confinement energy by Eq. (1). The confinement energy of the lowest electron level E_0 is estimated from the self-consistent eight-band $\boldsymbol{k}\cdot\boldsymbol{p}$ model.[43] The lowest electron and highest hole levels $E^+_{0,0}$ and $H^-_{0,0}$ at 3 T are estimated by inclusion of the Zeeman spin splitting term and using the band-edge masses for the spin up (+) and spin down (−) electron and hole, respectively. Using these approximations, the effect of type-I nonparabolicity on electron effective mass is plotted against the well width W in Fig. 5 as a dashed line. For comparison we plot the experimental data from the well width series as solid circles in the same graph. The mass enhancement observed in the well width series is substantially larger than predicted by type-I nonparabolicity. This suggests that as expected additional type-II nonparabolicity is very important.

The type-II nonparabolic mass is strongly dependent on the relative positions of the minigap and the Fermi energy E_F, whose value is affected by the additional hole charges in the system. In order to model a systematic behavior with well width we made the assumption that N_e/N_h=3/2 which allows us to calculate the Fermi energy using k^2_{Fe}/k^2_{Fh}=3/2 and $E_C(k_{Fe})=E_C(k_{Fh})=E_F$ in the conduction-band dispersion relation. This approximation assumes that the system is always semimetalic and n type. Although there is some change in N_e/N_h in the well width series, particularly for very narrow wells, a constant value N_e/N_h=3/2 is broadly consistent with the transport measurements of carrier densities in most samples (i.e., W=240 Å). Figure 4 shows the estimated variation of E_F for different cases of well width using this assumption. The asterisks marked on the dispersion relations in the left-hand panel show the point (k_{Fe},E_F) for each well width. In order to maintain the density ratio constant, E_F must increase with increasing electron confinement energy. The electron effective mass is dependent on the gradient of E_C at the point (k_{Fe},E_F). The closer k_{Fe} is to the minimum of E_C the larger the effective mass becomes. As the well narrows, its electron confinement energy increases rapidly and the electron level approaches the top of the hole band in the GaSb barrier.

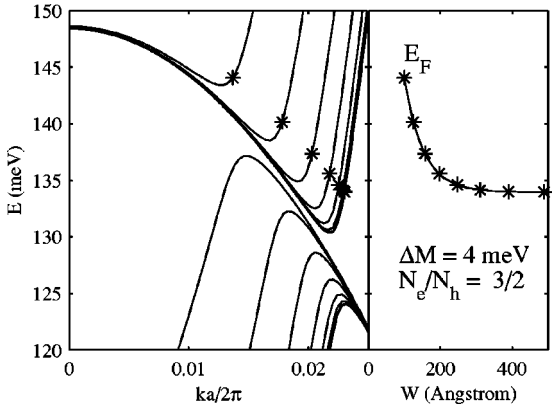

FIG. 4. Calculated values of the Fermi energy for different well widths. An electron/hole density ratio N_e/N_h=3/2 is assumed.

In Fig. 5 the effective mass is shown calculated using the coupled two-band model using both type-II nonparabolicity alone and including both the type-I and type-II contributions together. This shows that the data can be well fitted using a value of ΔM=4 meV. This value is consistent with the theoretical prediction of minigap values,[43] our own eight-band $\boldsymbol{k}\cdot\boldsymbol{p}$ calculation on bilayer structures and the experimental values measured for superlattices.[44]

2. Spacer series

As samples in the spacer series have constant well width, the confinement energies are almost constant, with a slight increase expected due to the increased confinement of the spacer layers. Effective mass variation in this series is therefore almost entirely due to the type-II nonparabolicity. Figure 6 shows the measured effective masses plotted against the number of superlattice periods at both interfaces. The effective electron mass of sample W60 is included as a comparison sample without any spacers. We observe that the addition of superlattice layers between electrons and holes at both interfaces reduces the cyclotron resonance mass sharply from $0.0378m_0$ (no superlattice) to $0.028m_0$ (ten superlattice peri-

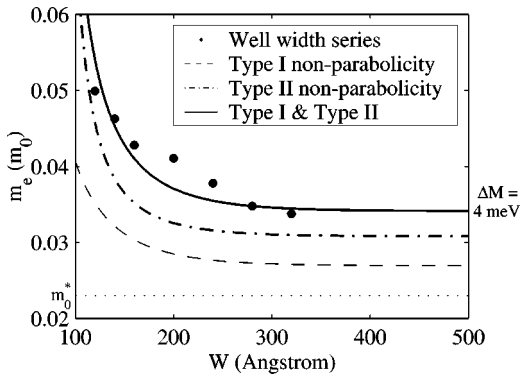

FIG. 5. Comparison of different nonparabolicity models to data from the well width series of samples (dots). Calculated masses m^*_e obtained from the hybridization model use ΔM=4 meV. The band-edge mass m^*_0 (dotted line) is included for comparison.

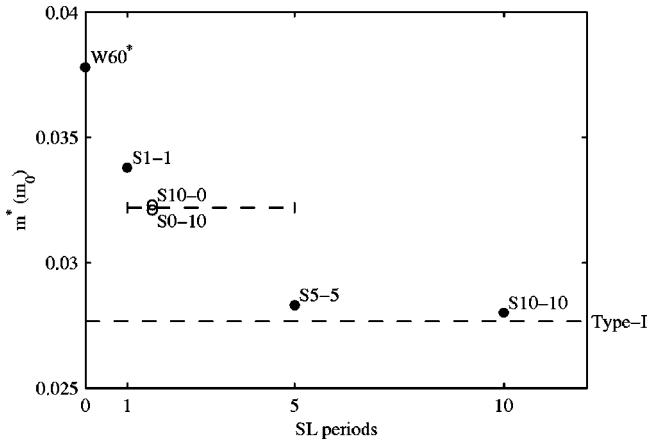

FIG. 6. Cyclotron resonance effective masses measured in spacer series samples are plotted against the number of superlattice periods at each side of the well. The mass of sample W60* is taken to represent a sample with no superlattice.

ods at each interface), which corresponds closely to the expected type-I nonparabolicity mass for this well width (dashed line). It is likely that the tunneling is much more strongly suppressed by the superlattice layers at the interfaces than possible electron-hole Coulomb interactions, and therefore the effect of type-II nonparabolicity at these interfaces is strongly reduced. It is evident that ten superlattice periods at both interfaces are enough to remove the type-II nonparabolicity effect completely, eliminating the minigap so that $\Delta M=0$. This conclusion is similar to the qualitative studies by[3,6,7,28] who demonstrated that the inclusion of an AlSb barrier with a thickness of order 2–4 nm was also enough to remove all evidence of electron-hole hybridization.

Samples S10-0 and S0-10 are shown indicatively in Fig. 6 as open circles. Although ten periods of superlattice at one interface would remove hybridization completely from that interface, hybridization at the other interface should be unaffected. This is consistent with the measured effective masses of S10-0 and S0-10 being approximately halfway between W60 and S10-10. The fact that the results from these two samples are so similar suggests that the structures are symmetric with both interfaces being very similar. Comparison with the other samples in the series then suggests that the addition of one to two periods of the superlattice is sufficient to halve the coupling strength.

C. Electron-hole hybridization at high field

At higher magnetic field ($B>3$T) oscillations observed in the resonance position, intensity, and linewidth are related to electron-hole Landau level hybridization. The magnetic field dependence of the resonance splits up into a series of lines which have a greater slope than the low-field behavior, but with intensities which gradually change within an overall envelope which follows the slope of the low-field mass. We also observe several weaker transition lines breaking away from the main electron cyclotron resonance line to the high-energy region, characteristic of interband transitions. The oscillations are associated with the anticrossing of the Landau levels, and it is in the vicinity of these anticrossing points that interband transitions become allowed. The interband transitions have much greater slope than the main cyclotron resonance line due to their smaller reduced effective masses. Strong coupling and multiple splittings from the main cyclotron resonance are clearly visible in the contour plot in Fig. 2(i) for the narrow well sample W40. It is seen that these transitions disappear to the high-energy side and are replaced by further transition lines entering from the low-energy side. This behavior is characteristic of initial state couplings,[11] and the three main coupling points are labeled as (α), (β), and (δ) for illustrative purposes.

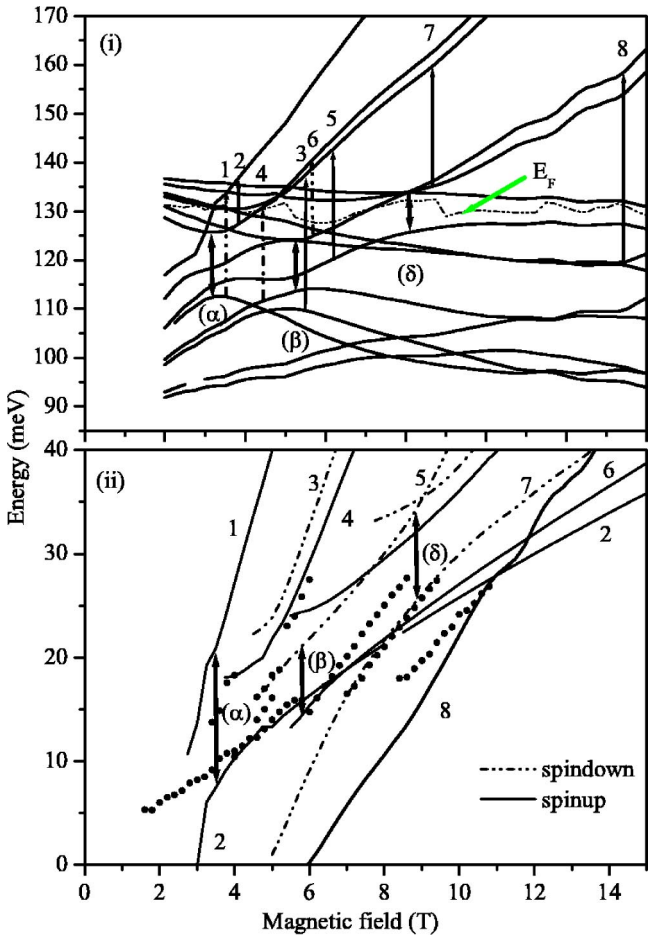

FIG. 7. Self consistent eight-band $\boldsymbol{k}\cdot\boldsymbol{p}$ modeling of the 160 Å InAs well (W40) for (i) electron and hole Landau levels and (ii) allowed electron-electron and electron-hole transitions. Some of the additional oscillations in the Landau levels are caused by the self-consistency and the consequent variations in carrier density with field. These oscillations do not affect the CR transitions significantly. Experimental data (solid circles) are shown taken from sample W40.

Self-consistent eight-band $\boldsymbol{k}\cdot\boldsymbol{p}$ calculations are performed on structures with varying InAs well width. An example of this is shown for the 160 Å well (W40) in Fig. 7. Resultant cyclotron resonance transitions of mixed Landau states $N\leqslant 3$ are calculated close to the anticrossing and are given the labels 1–8 as shown in Fig. 7(ii). The results of this calcu-

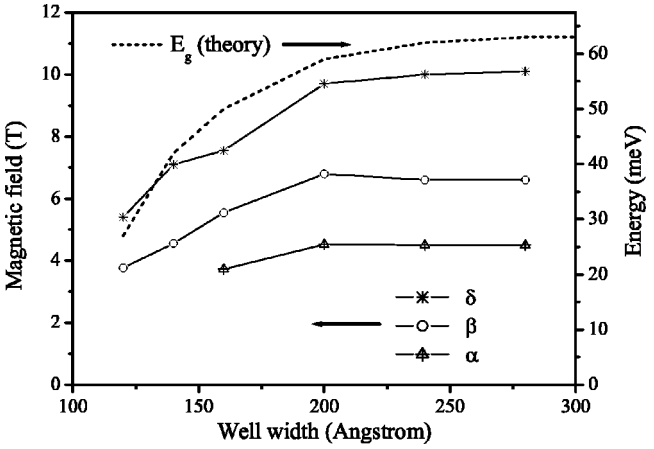

FIG. 8. Comparison between the theoretical value of the band gap (meV) and the magnetic field values (T) of the electron-hole hybridisation points δ, β, α.

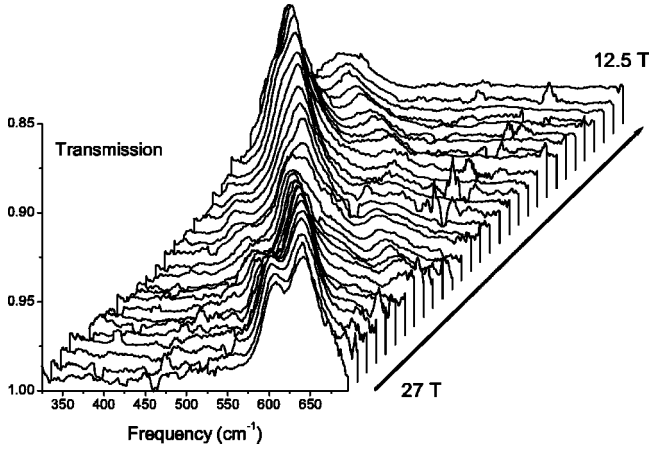

FIG. 9. Experimental high-field cyclotron resonance absorption in the quantum limit for sample W40. The relative transmission spectra are taken with a 0.5 T interval and offset in both x and y directions for clarity.

lation are in broad agreement with those reported previously by Tsay *et al.*[10] who suggest that there should be two main series of peaks with an energy splitting which is approximately constant with field. The strongest resonances from the data taken from sample W40 are also shown in Fig. 7 which shows that although there are well resolved split levels, with a splitting comparable to that predicted, the dominant transitions are centered around the lower branch formed from the transitions labeled 2, 6, and 7. The theory does predict transition features which are seen to split from the electron cyclotron resonance to the high energy with different slopes, similar to that observed in the experiments. It is evident that these transitions are due to the interband coupling between the electron and hole Landau levels. Both theoretical and experimental results show a continuous transformation of cyclotron resonance transitions into interband transitions consistent with their common selection rules $\Delta n = \pm 1$.[5,6,11]

Figure 8 shows a simple comparison between the zero field band overlap gap E_g (defined as the difference in energy between the lowest electron level and the highest hole level as deduced from $\boldsymbol{k}\cdot\boldsymbol{p}$ calculations) and experimental values of the fields corresponding to the electron-hole hybridization points (α), (β), and (δ), as a function of InAs well width. These points shift to higher magnetic field with increasing well width and follow quite well the value of E_g deduced from the $\boldsymbol{k}\cdot\boldsymbol{p}$ model, confirming the electron-hole Landau level hybridization as the source of the coupling. We note that the small discrepancy between theoretical and experimental results may be a result of errors arising from the estimation of the sample well widths from the growth rates.

By contrast to the other samples, in sample S10−10 the couplings and splittings are completely removed and the transmission spectra are dominated by a single electron cyclotron resonance at all fields. As concluded from the low-field mass values the additional ten-period superlattice at each interface removes all observable effects of hybridization. For the single side decoupled samples S10-0 and S0-10 (not shown here) weaker coupling features are observed at similar magnetic field values suggesting that the coupling is occurring in a similar way at both interfaces and that there is no evidence of any additional asymmetry in the structures.

D. Electron-hole hybridization in the quantum limit

In order to be more quantitative in the assignment of the cyclotron resonance transitions observed, a separate study was made of the cyclotron resonance in the quantum limit above the Reststrahlen band of the GaAs substrate, using steady magnetic fields from 11 to 27 T. Figures 9 and 10 show sets of spectra for samples W40 and S0-10 taken by ratioing the transmission with the transmission of an equivalent substrate measured at the same magnetic field. These two samples are typical of the results observed for the strongly coupled samples (W35−W60) and the weakly coupled structures (W70−S10-0). By contrast to the above results, the decoupled sample S10-10 shows a single resonance over almost the entire field range with only one small

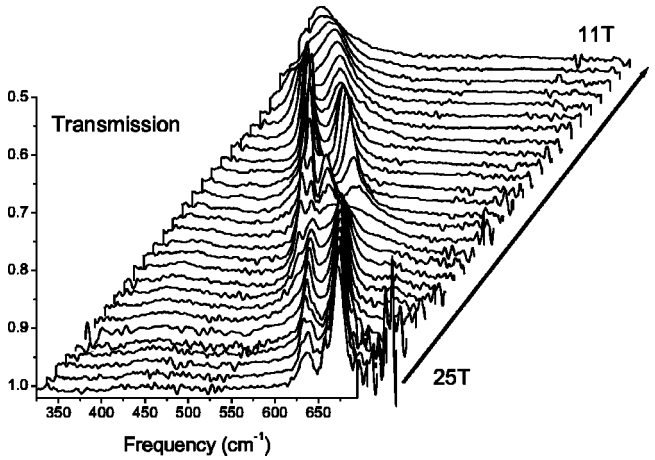

FIG. 10. Experimental high-field cyclotron resonance absorption in the quantum limit for sample S0-10. The relative transmission spectra are taken with a 0.5 T interval and offset in both x and y directions for clarity.

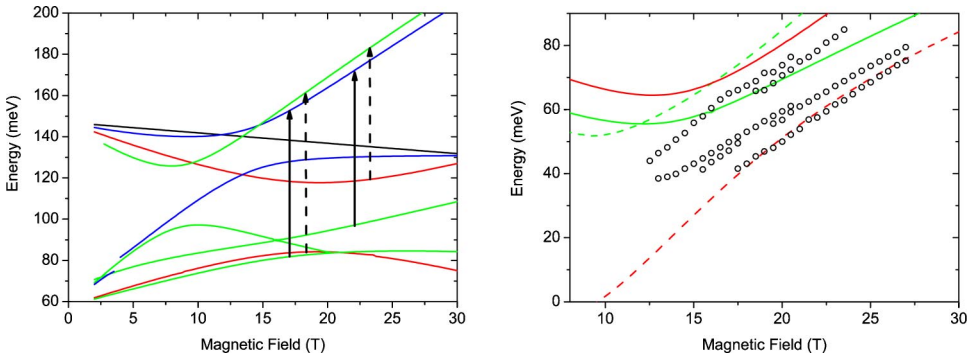

FIG. 11. Calculated Landau levels (left) and cyclotron resonance transitions (right) for a symmetric InAs/GaSb superlattice. The CR tranistions originating at spin-up and spin-down levels are shown as solid and dashed lines, respectively. The data points show the resonance positions deduced from the spectra shown in Fig. 9 for sample W40.

(final state) anticrossing in the region of 18 T which may be associated with some coupling to a higher confined electron state.

The spectra, which are taken in the quantum limit where the Landau level occupancy $\nu < 2$, should result from carriers only in the two spin states of the lowest electron Landau level. They nevertheless show a number of features which depend strongly on both the magnetic field and the well width. In particular the narrower well structures often show two dominant transitions split by over 100 cm^{-1} (12 meV) in the field range 12–20 T (e.g., Fig. 9), whereas by 27 T all samples show a pair of resonances which are split by 32–40 cm^{-1} (4–5 meV). In the quantum limit we would expect to only see two resonances from the lowest two electron levels and so we can interpret these as spin split cyclotron resonance which has been enhanced due to the coupling of the electron and hole Landau levels. The splitting of the line into multiple transitions is however surprising and in order to interpret the spectra we have again performed simple eight-band $\boldsymbol{k}\cdot\boldsymbol{p}$ calculations. In this case no self-consistency is used, in order to simplify the field dependence of the levels. The results of the calculations are shown in Figs. 11 and 12, where a few of the lowest Landau levels and cyclotron resonance transitions are shown compared to the data from samples W40 and S0-10. The calculations show at least four possible transitions originating from the coupled electron and hole levels of the lowest electron Landau level, but the calculations are strongly dependent on the structure which is modeled. Two calculations were made using two different assumptions. In the first the sample was assumed to consist of a symmetric superlattice structure with coupling occurring at both InAs/Gasb interfaces. In the second an electric field was applied across the two layers in order to simulate an asymmetric bilayer with coupling only at one interface. It can be seen that the theoretical results for the two cases are very different. For the asymmetric case the anticrossing of the lowest electron Landau level with the hole states is clear, with an anticrossing gap of order 10 meV for both spin states. In the symmetric structure the anticrossing gap is larger (of order 10–30 meV) and is also very different for the two different spin states. This is due to two effects, first, the obviously smaller coupling between the electrons and holes caused by the presence of only one interface and second, the additional confinement caused by the presence of the electric field which has the effect of moving the light hole levels away from the energy range where coupling occurs. When the light hole states take part in the coupling the spin-down electron states show significantly larger anticrossing effects, whereas the physically antisymmetric quantum well has very similar anticrossing behavior for spin-up and spin-down electrons. As a result the cyclotron resonance transition energies (Fig. 12) show much smaller spin splittings.

It can be seen that in practice the symmetric picture provides a reasonable description of the data for W40 in the field range 15–20 T, with several transitions being plotted all of which originate from the mixed electron and hole levels associated with the lowest electron Landau level. The strong spin dependence of the mixing leads to the appearance of giant spin splitting effects in this region, with the predicted splitting between the two transitions originating on the high field branches of the lowest Landau level being of order 20 meV. By contrast above 22 T and for the whole field range in the deliberately asymmetric sample S0-10 the spin splittings are much smaller (4–5 meV) and are very similar to those predicted (~meV) for the asymmetric structure as shown in Fig. 12. This difference in behavior is a strong evidence that even relatively simple single-particle mixing

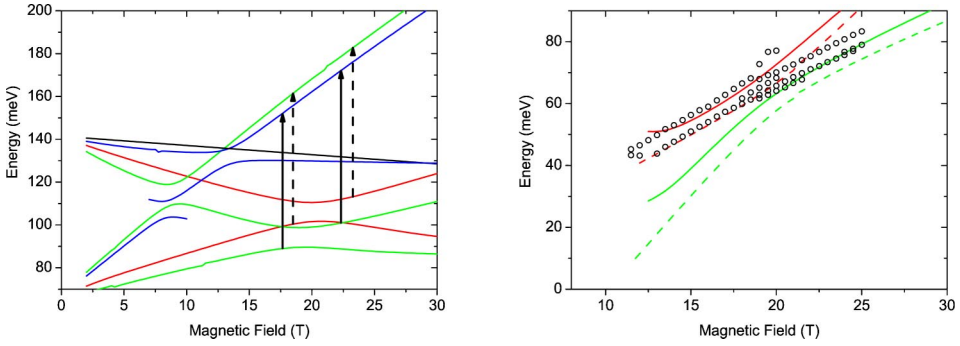

FIG. 12. Calculated Landau levels (left) and cyclotron resonance transitions (right) for an asymmetric InAs/GaSb superlattice. The CR transitions originating at spin-up and spin-down levels are shown as solid and dashed lines, respectively. The data points show the resonance positions deduced from the spectra shown in Fig. 10 for sample S0–10.

can have a dramatic effect on the cyclotron resonance behavior. One further factor that may influence the behavior is that some mixing is thought to occur with the lowest spin-down hole level which is thought not to mix in the simple axial $\boldsymbol{k}\cdot\boldsymbol{p}$ approach. The valence band anisotropy is likely to introduce a coupling to this state which is thought to be responsible for the sharp series of anticrossings occurring at around 20 T in both samples.

One surprising feature of the high-field results ($B>24$ T) is that the dominant transitions at high fields for the symmetric sample remain the lower energy resonances. These should originate at the upper spin state which should be emptying by these fields as all of the structures studied are approaching the absolute quantum limit ($\nu<1$) at this point. This suggests that the simple single-particle picture presented here is not complete, and further account should be taken of possible electron-electron plasma interactions which can modify the resonance behavior.[45–49] This interaction is known in particular to alter the relative intensities of spin split cyclotron resonances.[50] Although the systematics of the electron-hole hybridization described earlier show that there is no need to introduce any electron-hole interaction to explain the behavior at intermediate fields a study of the temperature dependence of the cyclotron resonance in this system suggests that electron-electron interactions can play an important role at much higher temperatures.[51]

V. CONCLUSION

In conclusion, we have demonstrated that the effects of electron-hole hybridization on InAs–GaSb structures are very significant, and that they can be controled in a consistent way by varying the structures studied. In the low-field limit the effective mass is additionally enhanced as a result of the type-II band nonparabolicity caused by the electron-hole coupling. The experimental findings can be fitted successfully by a simple two-band model with a minigap size of 8 meV. The use of superlattice spacer layers between the electrons and holes shows that the coupling can be rapidly reduced thus reducing the mass. At intermediate fields, a series of splittings is observed which depart from the simple-electron cyclotron resonance line at the point where the electron and hole Landau levels anticross. These are attributed to the appearance of interband transitions which become more strongly allowed where the states mix. The insertion of spacer layers between the electrons and holes removes all these effects. The field positions of the couplings are strongly influenced by the electron confinement energies in a way which is broadly consistent with calculations based on a theoretical $\boldsymbol{k}\cdot\boldsymbol{p}$ model. In the high-field limit the electron-hole coupling can lead to the appearance of multiple cyclotron resonances and giant spin splittings.

*Current address: Department of Physics, Thammasat University, Klongluong, Phatumtani 12121 Thailand.
†Current address: NTT Basic Research Laboratories, 3-1 Morinosato Wakamiya, Atsugi-shi, Kanagawaken 243-0198, Japan.

[1] D. Heitmann, M. Ziesmann, and L. L. Chang, Phys. Rev. B **34**, 7463 (1986).
[2] J.-P. Cheng, J. Kono, B. D. McCombe, I. Lo, W. C. Mitchel, and C. E. Stutz, Phys. Rev. Lett. **74**, 450 (1995).
[3] J. Kono, B. D. McCombe, J.-P. Cheng, I. Lo, W. C. Mitchel, and C. E. Stutz, Phys. Rev. B **55**, 1617 (1997).
[4] J.-C. Chiang, S.-F. Tsay, Z. M. Chau, and I. Lo, Phys. Rev. Lett. **77**, 2053 (1996).
[5] S. D. Suchalkin, Y. B. Vasilyev, K. von Klitzing, V. N. Golovach, G. G. Zegrya, S. V. Ivanov, P. S. Kop'ev, and B. Y. Meltser, JETP Lett. **68**, 792 (1998).
[6] Y. Vasilyev, S. Suchalkin, K. von Klitzing, B. Meltser, S. Ivanov, and P. Kop'ev, Phys. Rev. B **60**, 10 636 (1999).
[7] T. P. Marlow, L. J. Cooper, D. D. Arnone, N. K. Patel, D. M. Whittaker, E. H. Linfield, D. A. Ritchie, and M. Pepper, Phys. Rev. Lett. **82**, 2362 (1999).
[8] S. DePalo, F. Rapisarda, and G. Senatore, Phys. Rev. Lett. **88**, 206401 (2002).
[9] S. de-Leon, L. D. Shvartsman, and B. Laikhtman, Phys. Rev. B **60**, 1861 (1999).
[10] S.-F. Tsay, J.-C. Chiang, Z. M. Chau, and I. Lo, Phys. Rev. B **56**, 13 242 (1997).
[11] C. Petchsingh, R. J. Nicholas, A. J. L. Poulter, V. J. Hales, N. J. Mason, and P. J. Walker, Physica E (Amsterdam) **6**, 660 (2000).
[12] E. D. Palik, G. S. Picus, S. Teitler, and R. F. Wallis, Phys. Rev. **122**, 475 (1961).
[13] G. Bastard, Phys. Rev. B **25**, 7584 (1982).
[14] U. Rössler, Solid State Commun. **49**, 943 (1984).
[15] F. Thiele, U. Merkt, J. P. Kotthaus, G. Lommer, F. Malcher, U. Rössler, and G. Weimann, Solid State Commun. **62**, 841 (1987).
[16] M. A. Hopkins, R. J. Nicholas, M. A. Brummell, J. J. Harris, and C. T. Foxon, Phys. Rev. B **36**, 4789 (1987).
[17] M. A. Hopkins, R. J. Nicholas, P. Pfeffer, W. Zawadzki, D. Gauthier, J. C. Portal, and M. A. DiForte-Poisson, Semicond. Sci. Technol. **2**, 568 (1987).
[18] U. Ekenberg, Phys. Rev. B **40**, 7714 (1989).
[19] R. J. Warburton, J. G. Michels, R. J. Nicholas, J. J. Harris, and C. T. Foxon, Phys. Rev. B **46**, 13 394 (1992).
[20] G. M. Sundaram, R. J. Warburton, R. J. Nicholas, G. M. Summers, N. J. Mason, and P. J. Walker, Semicond. Sci. Technol. **7**, 985 (1992).
[21] B. R. Nag and S. Mukhopadhyay, Phys. Lett. A **166**, 395 (1992).
[22] G. Bastard, *Wave Mechanics Applied to Semiconductor Heterostructures* (Les Editions de Physique, Les Ulis, France, 1988).
[23] M. J. Yang, P. J. Lin-Chung, B. V. Shanabrook, J. R. Waterman, R. J. Wagner, and W. J. Moore, Phys. Rev. B **47**, 1691 (1993).
[24] P. Bruelemans, P. Janssen, H. Schets, G. Borghs, and J. Witters, Solid State Commun. **105**, 513 (1998).
[25] C. Petchsingh, R. J. Nicholas, K. Takashina, N. J. Mason, and J. Zeman, Physica E (Amsterdam) **12**, 289 (2002).
[26] R. J. Nicholas, Y. Shimamoto, Y. Imanaka, N. Miura, N. J. Mason, and P. J. Walker, Solid-State Electron. **40**, 181 (1996).
[27] D. J. Barnes, R. J. Nicholas, R. J. Warburton, N. J. Mason, P. J. Walker, and N. Miura, Phys. Rev. B **49**, 10 474 (1994).

[28] J. H. Roslund, K. Saito, K. Suzuki, H. Yamaguchi, and Y. Hirayama, Jpn. J. Appl. Phys., Part 1 **39**, 2448 (2000).
[29] M. Lakrimi, S. Khym, R. J. Nicholas, D. M. Symons, F. M. Peeters, N. J. Mason, and P. J. Walker, Phys. Rev. Lett. **79**, 3034 (1997).
[30] C. R. Pidgeon, D. L. Mitchell, and R. N. Brown, Phys. Rev. **154**, 737 (1967).
[31] C. C. Chang, D. Phil. thesis, University of Oxford, 1998.
[32] M. Altarelli, J. C. Maan, L. L. Chang, and L. Esaki, Phys. Rev. B **35**, 9867 (1987).
[33] C. Nguyen, B. Brar, H. Kroemer, and J. H. English, Appl. Phys. Lett. **60**, 1854 (1992).
[34] J. Singleton, *Band Theory and Electronic Properties of Solids* (Oxford University Press, Oxford, 2001).
[35] K. W. Chiu, T. K. Lee, and J. J. Quinn, Surf. Sci. **58**, 182 (1976).
[36] T. A. Kennedy, R. J. Wagner, B. D. McCombe, and J. J. Quinn, Solid State Commun. **18**, 275 (1976).
[37] D. A. Allwood, N. J. Mason, and P. J. Walker, J. Cryst. Growth **195**, 163 (1998).
[38] P. C. Klipstein, S. G. Lyapin, N. J. Mason, and P. J. Walker, J. Cryst. Growth **195**, 168 (1998).
[39] K. Takashina, D. Phil. thesis, University of Oxford, 2002.
[40] K. Takashina, R. J. Nicholas, B. Kardynal, N. J. Mason, D. K. Maude, and J. C. Portal, Physica B **298**, 8 (2001).
[41] K. Takashina, R. J. Nicholas, B. Kardynal, N. J. Mason, D. K. Maude, and J. C. Portal, Phys. Rev. B **68**, 235303 (2003).
[42] Y. B. Vasilyev, S. D. Suchalkin, S. V. Ivanov, P. S. Kop'ev, B. Y. Meltser, and K. von Klitzing, JETP Lett. **69**, 343 (1999).
[43] M. Altarelli, Phys. Rev. B **28**, 842 (1983).
[44] A. J. L. Poulter, M. Lakrimi, R. J. Nicholas, N. J. Mason, and P. J. Walker, Phys. Rev. B **60**, 1884 (1999).
[45] J. Appel and A. W. Overhauser, Phys. Rev. B **18**, 758 (1978).
[46] N. R. Cooper and J. T. Chalker, Phys. Rev. Lett. **72**, 2057 (1994).
[47] B. E. Cole, F. M. Peeters, A. Ardavan, S. O. Hill, J. Singleton, W. Batty, J. M. Chamberlain, A. Polisskii, M. Henini, and T. Cheng, J. Phys.: Condens. Matter **9**, 3163 (1997).
[48] B. E. Cole, W. Batty, J. Singleton, J. M. Chamberlain, L. Li, L. van Bockstal, Y. Imanaka, Y. Shimamoto, N. Miura, F. M. Peeters, M. Henini, and T. Cheng, J. Phys.: Condens. Matter **9**, 4887 (1997).
[49] K. Asano and T. Ando, Phys. Rev. B **58**, 1485 (1998).
[50] J. G. Michels, M. S. Daly, P. Gee, S. Hill, R. J. Nicholas, J. Singleton, G. M. Summers, R. J. Warburton, C. T. Foxon, and J. J. Harris, Phys. Rev. B **54**, 13807 (1996).
[51] C. Petchsingh, R. J. Nicholas, K. Takashina, and N. J. Mason, Phys. Rev. B (submitted).